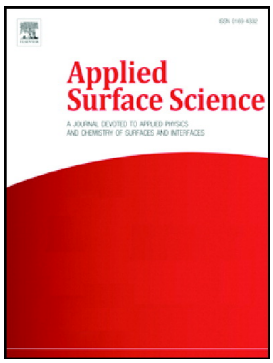

Lanthanum (oxy)boride thin films for thermionic emission applications

A. Bellucci, M. Mastellone, S. Orlando, M. Girolami, A. Generosi, B. Paci, P. Soltani, A. Mezzi, S. Kaciulis, R. Polini, D.M. Trucchi

PII: S0169-4332(19)30261-2
DOI: https://doi.org/10.1016/j.apsusc.2019.01.230
Reference: APSUSC 41629

To appear in: *Applied Surface Science*

Received date: 12 November 2018
Revised date: 22 January 2019
Accepted date: 25 January 2019

Please cite this article as: A. Bellucci, M. Mastellone, S. Orlando, et al., Lanthanum (oxy)boride thin films for thermionic emission applications, Applied Surface Science, https://doi.org/10.1016/j.apsusc.2019.01.230

Lanthanum (oxy)boride thin films for thermionic emission applications

A. Bellucci[1,2,*], M. Mastellone[1,3], S. Orlando[2], M. Girolami[1], A. Generosi[4], B. Paci[4], P. Soltani[5], A. Mezzi[5], S. Kaciulis[5], R. Polini[1,6], and D. M. Trucchi[1]

[*]alessandro.bellucci@ism.cnr.it

.

[1] DiaTHEMA Lab, Istituto di Struttura della Materia (ISM-CNR) Sez. Montelibretti, Via Salaria km 29.300, Monterotondo Scalo (RM), 00015, Italy.
[2] Istituto di Struttura della Materia (ISM-CNR) Sez. Tito Scalo, Contrada Santa Loja, Tito Scalo (PZ), 85050, Italy
[3] Dipartimento di Scienze di Base ed Applicate per l'Ingegneria, Università di Roma "La Sapienza", Via A. Scarpa 14, Rome, 00161, Italy.
[4] Istituto di Struttura della Materia (ISM-CNR), Via del Fosso del Cavaliere 100, Roma, 00100, Italy.
[5] Istituto per lo Studio dei Materiali Nanostrutturati (ISMN-CNR), Via Salaria km 29.300, Monterotondo Scalo (RM), 00015, Italy.
[6] Dipartimento di Scienze e Tecnologie Chimiche, Università di Roma “Tor Vergata”, Via della Ricerca Scientifica 1, Rome, 00133, Italy

Keywords: Thermionic emission; low work function; lanthanum borides; Pulsed Laser Deposition; electron beam evaporation.

Abstract

The chemical-physical properties of thin lanthanum (oxy)boride films deposited on polycrystalline tantalum substrates by different deposition techniques (Pulsed Laser Deposition with either nanosecond or femtosecond laser source, and electron beam evaporation) were compared in order to investigate the effect of chemical composition, crystallinity, surface morphology of the thin films on the thermionic electron emission capability. The emission performance of the films was analyzed in the 700 - 1600 °C temperature range, allowing the determination of work function values ranging from 2.59 to 2.85 eV and an effective Richardson constant at least one order of magnitude lower than the ideal value for all the films. The highest measured thermionic current density value of 1.68 A/cm^2 at 1600 °C was provided by the samples grown by femtosecond PLD, indicating a promising performance for practical application in high-temperature thermal-to-electric energy conversion.

1. Introduction

High-temperature (>1000 °C) solid-state thermal-to-electrical energy conversion relies mainly upon the development of efficient thermophotovoltaic (TPV) [1] or thermionic (TI) [2] devices. Different approaches have been introduced for lowering the operating temperatures with acceptable conversion efficiency values: thermoelectric [3] and combined thermionic-thermoelectric [4, 5] generators, photon-enhanced thermionic emission devices [6, 7, 8]. Another approach is to maximize the efficiency and the output instantaneous power density for ultra-high temperature (>1400 °C) sources, which, on the other hand, are interesting for the capability of driving chemical energy storage systems. This is the case of an extremely novel conceptual device is a hybrid TI and TPV solid-state converter proposed as thermionic-photovoltaic (TIPV) generator [9]. In TIPV, one of the most important challenge is the fabrication of a low work-function thermionic cathode operating stably and reliably at such temperatures.

In particular, the fabrication of an efficient TIPV converter allows for the exploitation of higher power density with respect to the single converters operating independently, since two mechanisms act in parallel: 1) the electron flux emitted by the TI cathode and collected by the anode generating an output power; 2) the photon flux emitted by the TI cathode and absorbed by the TPV cell, generating another output power. It appears clear that the TI cathode within the TIPV device has to efficiently emit both electrons and photons. To do this, it must have: high melting point, far higher than the operating temperature, and high thermal stability; very low electric resistivity (10^{-4} - 10^{-5} Ω cm) to avoid bottlenecks for electron refilling from the external circuit (or, alternatively, to ensure a low cathode series resistance); work function ϕ_C as low as possible, but at the same time higher than the anode's one ϕ_A ($\phi_C > \phi_A$) to ensure the proper power generation; spectrally selective emissivity matched with the photovoltaic cell, i.e. high (low) emissivity for wavelengths smaller (larger) than the wavelength corresponding to the bandgap of the PV cell active material.

Aimed at meeting all these requirements, we propose a cathode structure composed of a refractory metal substrate, such as tungsten (W) or tantalum (Ta), and an emitting thin layer of lanthanum hexaboride (LaB_6), well known in modern technology as an outstanding thermionic electron emission source, thanks to its low work function, the high melting point (2600 °C), the low volatility at high temperatures, and the excellent chemical stability [10]. The thin-film approach discussed here aims at minimizing the production costs with respect to the use of a single-crystal LaB_6 bulk cathode, especially for the large area applications.

The thermionic emission capability is measured according to two physical parameters: the work function, which must be as low as possible, and the Richardson constant, which must be as close as

possible to the ideal value of 120 A cm^{-2} K^{-2} and depends on the physical properties of the involved materials [11].

According to the literature, LaB_6 single-crystal demonstrates a large susceptibility to the internal La/B ratio and to the surface oxidation, which in turn depends on the amount of dangling bonds that are available for sticking oxygen and, consequently, on the single-crystal orientation [12]. These factors lead to different values of work function, from 2.4 eV for (001) to 3.4 eV for (111) surfaces. Moreover, the natural oxidation process increases the work function from 2.3 eV up to 4.0 eV depending on the oxygen exposure. Therefore, polycrystalline thin films have an average value of work function resulting from the exposed crystallographic planes present in the film structure. In literature, the values of work function ranging from 2.6 to 3.4 eV were reported for thin films deposited by different techniques, such as thermal evaporation [13], magnetron sputtering [14], and Pulsed Laser Deposition (PLD) [15]. In any case, the properties of the films can depend on parameters differing as a function of the growth mechanism: the surface roughness of the substrate, composition of bulk target, vacuum conditions, etc.

Herewith we present a systematic study, based on the analysis and comparison of lanthanum (oxy)boride thin films deposited by different growth techniques aimed at finding the best thermionic emission capability in the temperature range 700 - 1600 °C, in order to verify the feasibility for integration in a hybrid TIPV conversion.

2. Experimental

Pulsed laser ablation of 1-inch diameter commercial target LaB_6 (purity 99.95%, produced by MaTecK GmbH) was performed by using two different laser sources impinging at 45° with respect to the surface target: ns-pulse ArF excimer laser (Lambda Physik COMPex 102, operating at 193 nm wavelength, 7 ns pulse duration, 10 Hz repetition rate, 75±3 mJ pulse energy); fs-pulse Ti:Sapphire laser (Spectra Physics Spitfire Pro XP, operating at 800 nm wavelength, pulse duration of 100 fs, repetition rate ranging from 10 to 1000 Hz, 3.7±0.1 mJ pulse energy).

Polycrystalline tantalum discs (10 mm diameter, 3 mm thickness) and (111) silicon single-crystal wafers, surface etched for removing native oxide and ultrasonically cleaned in n-hexane before being placed on the substrate holder, were used as deposition substrates.

In both ns- and fs-PLD, the vacuum chamber was initially evacuated down to 5.0×10^{-7} mbar base pressure by using a turbomolecular pump, the substrates were mounted on a holder facing the target at a distance of 50 mm, and the laser beam was focused on the target plane. During the deposition, the target was continuously rotated to ensure uniform erosion over the surface. The substrate holder

of fs-PLD cannot be heated, consequently the deposition temperature was close to room temperature (RT). Conversely, in ns-PLD the substrate temperature was changed from 300 to 600 °C with steps of 100 °C, for the different sets of depositions. In this case, immediately after the deposition, the samples were maintained at the temperature for 3 hours and then slowly cooled down to room temperature at a rate of 2 °C/min.

The electron beam (e^--beam) deposition system was used at acceleration voltage and emission current of 8.3 kV and 150 mA, respectively, for the evaporation of LaB_6 pellets, obtained by breaking mechanically the LaB_6 target used for PLD, contained in a tungsten crucible. Also in this case, before starting the deposition, the chamber was evacuated down to 5.0×10^{-7} mbar.

The surface morphology of the deposited films was observed by field emission gun scanning electron microscopy (FEG-SEM, LEO Supra 35), equipped for energy dispersive X-ray spectroscopy (EDS, Oxford Instruments mod. INCA 300).

X-ray diffraction measurements (XRD) were performed in reflection mode on a Panalytical Empyrean Diffractometer, using the Kα fluorescence line of a Cu-anode emitting tube as X-ray probe. A Bragg Brentano divergent configuration was chosen as incident optical pathway and a solid-state hybrid Pix'cel 3D detector, working in 1D linear mode, accomplished the detection. A wide angular range was explored ($10° < 2\vartheta < 110°$).

Raman measurements were performed by means of a Renishaw In-Via spectrometer, mounting a 457 nm laser in standard confocal mode. The experimental setup was optimized: 2400 cm/line grid with a 100X optical magnification, laser power at 5% of its maximum intensity and 50 accumulations for t = 10 s/point for each data acquisition. Same experimental conditions were kept for all measured samples.

X-ray (XPS) and Ultraviolet (UPS) Photoelectron Spectroscopies were carried out by using an ESCALAB 250 Xi (Thermo Fisher Scientific, UK), equipped with a monochromatized Al Kα and ultraviolet He (21.2 and 40.8 eV) sources, and a 6-channeltron spectroscopic detection system. XPS measurements were carried out at 90° take-off angle and standard electromagnetic lens mode, resulting in 1 mm diameter of analyzed sample area. The UPS measurements were carried out at a pressure of about 2×10^{-8} and 5×10^{-9} mbar for He I and II lines, respectively. The spectra were collected at 2 eV pass energy before and after a very short surface cleaning by ion sputtering. The work function ϕ of the samples was calculated by measuring the characteristic cut-off energy in the He I spectrum. Spectroscopic data were acquired and processed by the Avantage v.5 software.

Shirley background subtraction and mixed Lorentzian/Gaussian peak shape (30%) were used for the peak fitting. Additional details are reported elsewhere [16].

The thermionic electron emission of deposited thin films was characterized in a custom made ultra-high vacuum (UHV) chamber. Once the sample was loaded into the vacuum chamber and pumped to a background pressure of 5×10^{-8} mbar, it was heated by a DC laser beam (808 nm) focused onto its backside surface. Pressure during measurement did not exceed 10^{-7} mbar. Temperature was measured by thermocouples placed inside the sample holder and by an optical pyrometer focusing the sample under test. Electrons emitted from the sample surface were collected by a cooled metallic anode positioned at a distance of 0.1 mm and biased in the range ±500 V for performing current-to-voltage characterization in steady-state conditions (i.e. constant temperature) by a Keithley 487 electrometer. A Pfeiffer Prisma (QM200 model) mass spectrometer, installed in the UHV chamber, was used for monitoring chemical species desorption during the measurements.

3. Discussion and results

3.1 Deposition of films by ns-PLD

Thin films deposited at different substrate temperatures (from 300 to 600 °C) by ns-PLD were previously developed on (111) single-crystal silicon substrates in order to evaluate the effects of the deposition temperature on crystallinity and stoichiometry of the resulting materials. The best recipe was successfully transferred on polycrystalline tantalum substrates, finding the same characteristics and suggesting that the properties of the resulting films do not depend on the substrate type. The structural analyses performed by XRD disclose the formation of crystalline oxide phases (lanthanum orthoborate, $LaBO_3$, and boron oxide, B_2O_3) without any signature of LaB_6, independently from the substrate temperature. In fact, **Figure 1** shows the XRD spectra for the films deposited at the temperature range extremes of 300 and 600 °C, the patterns of which are perfectly overlapping and only $LaBO_3$ [17] and B_2O_3 [18] peaks are detected.

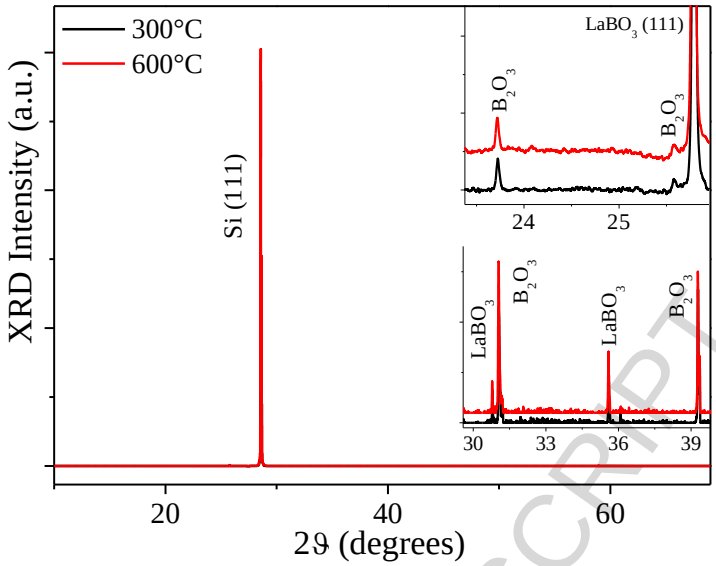

Figure 1: XRD spectra of the thin films deposited at 300 and 600 °C. The samples obtained at intermediate temperatures show similar patterns.

The effect of deposition temperature both on peak positions and linewidths were evaluated: no variations were observed for these two parameters, thus proving that no stresses nor modification of the crystallite grain-size were induced on the film. Raman patterns were collected on all samples, however no information could be gained regarding the films deposited on silicon substrates at different deposition temperatures, due to the Si modes strongly dominating the whole region of interest. Chemical composition of the samples was investigated by XPS. **Figure 2a** shows a typical B 1s spectrum, where it is possible to distinguish the contributions of oxy-borides and borides. The O 1s and La $3d_{5/2}$ spectra are shown in **Figure 2b** and **2c**, respectively**.** Contrarily to the B 1s deconvolution, the identification of La species by the peak-fitting of La 3d spectrum is complicated due to the presence of strong shake-up satellite and plasmon peaks [19].

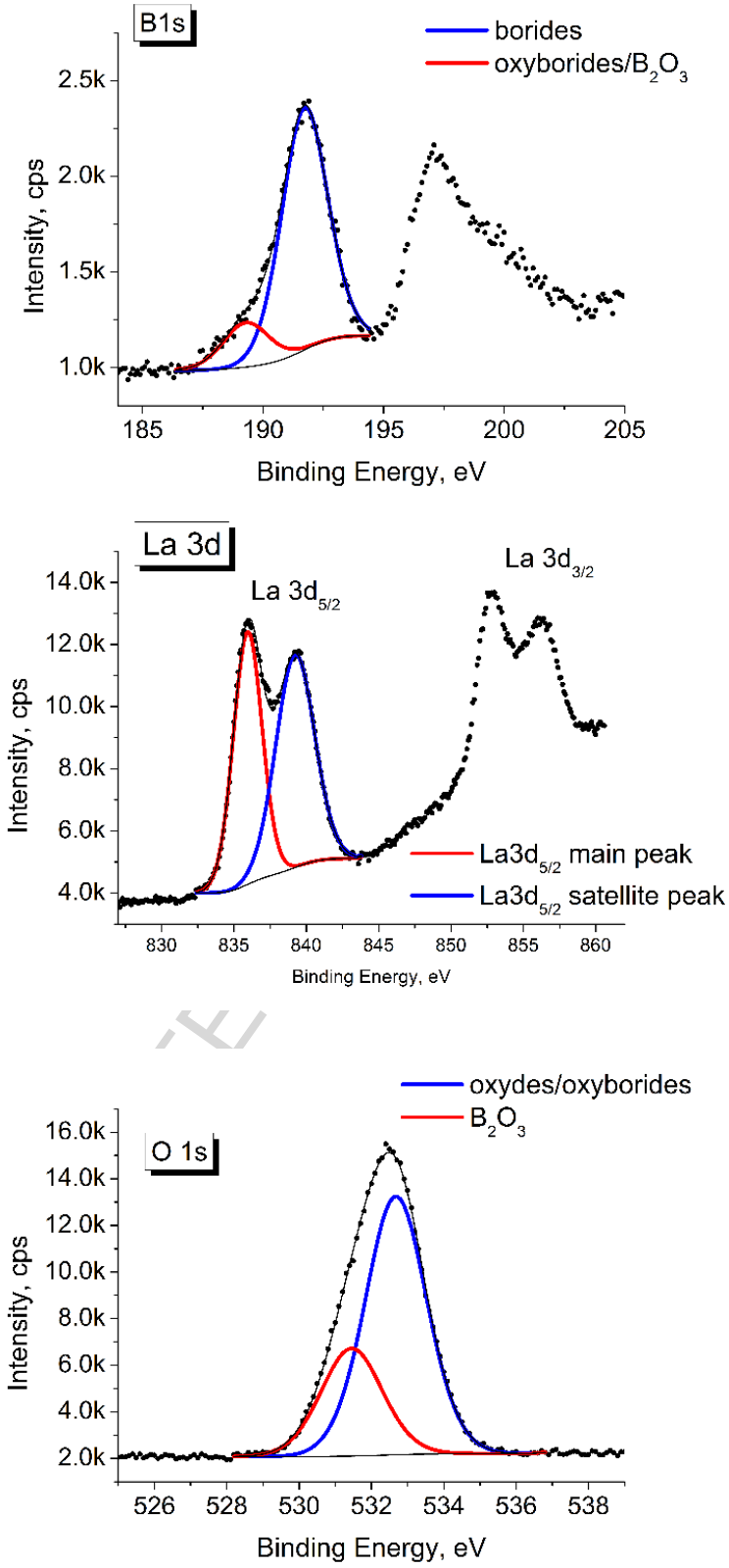

Figure 2: Peak fitting of a) B 1s, b) La $3d_{5/2}$, c) O 1s spectra for the thin film deposited at 300 °C (similar spectra were obtained at the different deposition temperatures).

The semi-quantitative analyses of these signals is shown in **Figure 3** that reports the atomic concentration ratios La/O, B/O and boride/oxyboride as a function of the deposition temperature,

inferred by XPS measurements. As it can be seen, there is a predominant presence of oxy-boride instead of boride content at every deposition temperature: this means that, even in the best case (boride-to-oxyboride ratio of 0.23), more than 80% of B atoms are bonded to oxygen. The oxygen content is high, with atomic ratio of La/O between 0.22 and 0.28, whereas the highest value of B/O ratio (0.74) is obtained for the sample deposited at 300 °C. It's worth mentioning that these data were recorded after the removal of the contamination layer, performed by Ar^+ ion sputtering, revealing that, in addition to the first oxidized layers formed by exposure of the films to the ambient atmosphere, a very high O content is present also in the films bulk.

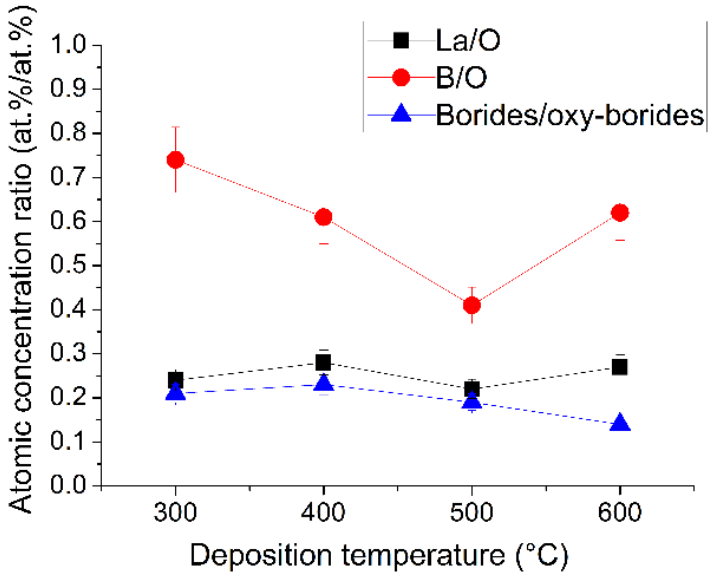

Figure 3: Atomic ratios of La/O, B/O and borides/oxy-borides as a function of the substrate deposition temperature.

By combining these information with the lack of a LaB_6 crystalline phase, it can be deduced that amorphous La-B oxygen-free compounds (about 15-20% with respect to oxy-borates, as indicated by XPS signals) is included in a polycrystalline matrix of oxy-borides.

Such a composition is quite unexpected was never reported in the literature [20, 21] for thin films grown by ns-PLD, which generally allows for the development of polycrystalline LaB_6 thin films with a low oxygen contamination. A residual vacuum chamber pressure of 5.0×10^{-7} mbar is not probably sufficient to prevent oxidation of either the target or the species present in the plume expansion and it could explain such different behavior. Indeed, the O atoms tend to replace B ones thus forming borate BO_3^{3-} structures, such as $LaBO_3$, or possible boron oxides, such as B_2O_3, as previously reported in literature with simulation and X-ray absorption near edge spectroscopy studies (XANES) [22].

3.2 Deposition of films by fs-PLD

Alternative technique is fs-PLD, that was used by our group for the deposition of LaB_6 for the first time [23] and here is discussed comparatively with the other deposition methods. With fs-PLD the growth dynamic is completely different from ns-PLD; indeed, fs-PLD induces a higher formation rate of nanoparticles, with a large reduction of thermal interactions and minimal modifications of the target composition and structure during the ablation [24]. **Figure 4** shows the XRD patterns and the Raman spectra provided by the samples deposited at a pulse repetition rate of 200 Hz onto polycrystalline tantalum substrates (ICDD:00-004-0788). Raman pattern is plotted in the 700-1700 cm^{-1} range to enhance only the detected significant contributions. LaB_6 peaks (ICDD: 96-110-1024, labelled in figure) and Raman modes are revealed by both techniques, without formation of oxides in crystalline structure. In particular, the detected Raman bands can be attributed to LaB_6 characteristic shifts: peaks at 1115 cm^{-1} and 1250 cm^{-1} match the Raman-active modes Eg and A1g of LaB_6. As regards the chemical composition, fs-PLD samples show La/O and B/O atomic ratios equal to 0.22 and 1.21, respectively, whereas the borides/oxyborides ratio is 3.3, namely at least one order of magnitude higher than the case of ns-PLD films. Moreover, conversely to the ns-PLD films, less than 25% of B atoms are bonded with oxygen.

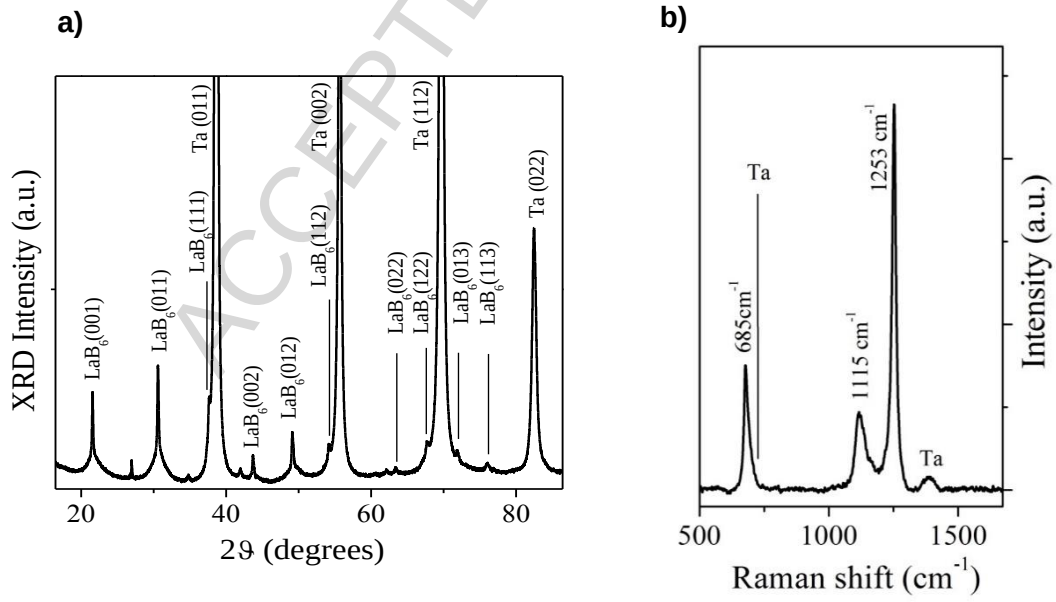

Figure 4: a) XRD and b) Raman spectra of the thin films deposited by fs-PLD.

3.3 Deposition of films by e^--beam evaporation

Samples deposited by electron beam evaporation show borides/oxyborides ratio of 5.9, measured by XPS, representing the highest value among the different developed samples. It emerges also that less than 15% of B atoms are bonded within oxy-borides. However, the ratios of La/O and B/O (0.19 and 0.85, respectively) are comparable to those recorded for films grown by ns-PLD, indicating that the oxygen incorporation remains still high but in compounds other than oxyborides.

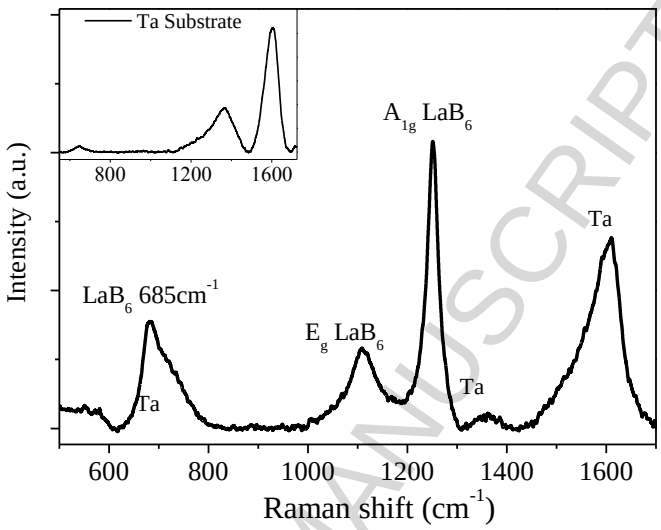

Figure 5: Typical Raman spectrum of thin films deposited on Ta substrates by electron beam evaporation.

No crystalline phases are revealed by XRD. However, Raman spectra confirm the presence of LaB_6 (Figure 5), suggesting that the compound deposited by e^--beam might be amorphous. In fact, as for fs-PLD samples, also in this case the Raman bands can be attributable to the presence of LaB_6, with, in addition, the detection of the band at 685 cm^{-1} that is characteristic of the LaB_6 samples. The amorphous nature of the films deposited by electron beam was already reported in the case of deposition at temperatures close to RT [10]. The amorphous structure of the films is furthermore confirmed by the slight downshift of the Raman bandwidth with respect to the pristine target. Most significantly, all the bands have significant high values of Full Width Half Maximum values (FWHM) typical for disordered material.

3.4 Comparison of films developed by the different techniques

In order to test the thermionic emission capability and perform a direct comparison among the samples deposited by the different techniques, the films with chemical-physical properties better approaching the ideal ones were selected. It is worth recalling that the material source (LaB_6 target),

the polycrystalline tantalum substrates with comparable surface roughness and composition, and the base vacuum pressure (5.0×10^{-7} mbar) were the same for the different samples. In **Table I** the main deposition parameters and films' characteristics are resumed before and after a soft sputtering for cleaning the surface (about 1 nm thickness of material removal), including the values of work function measured at RT by UPS. It is interesting to notice that the boride content increases after surface cleaning for all the analyzed samples.

Deposition technique	**Substrate temperature (°C)**	**Detected crystalline species**	**Boride content in as grown samples (%)**	**Boride content after sputtering (%)**	**ϕ of as grown sample (eV)**	**ϕ after sputtering (eV)**
ns-PLD	300	$LaBO_3$, B_2O_3	10.6	16.7	3.4	3.3
fs-PLD	RT	LaB_6	79.1	86.9	3.4	3.2
e^--beam evaporation	RT	Amorphous	70.1	85.5	3.6	3.4

Table I: Deposition parameters and physical properties of the developed films deposited by the different techniques. The percentage of borides was determined from the peak fitting of B 1s XPS core level spectra. The work function ϕ was measured by UPS before and after 30 s of Ar^+ ion sputtering for surface cleaning (≈1 nm).

Specifically, the atomic ratios of constituent elements before and after ion sputtering are reported in **Figure 6**. The oxygen content is higher in the ns-PLD samples, but it is significant also in the samples deposited by the two other techniques, independently from the removal of the outmost oxidized surface layers. XPS depth profiles (not shown) of fs-PLD and of e^--beam samples reveal that the thickness of the oxidized surface layer (i.e. the layer over which the oxygen signal becomes null) is 25±5 nm, that is far larger than the layer thickness removed by ion sputtering. The presence of the oxide layer is expected to be detrimental for achieving a low work function. Indeed, UPS measurements reveal work function values ranging from 3.4 to 3.6 eV for all the as-grown samples, with a small reduction of 0.1 – 0.2 eV after the removal of the outmost layer.

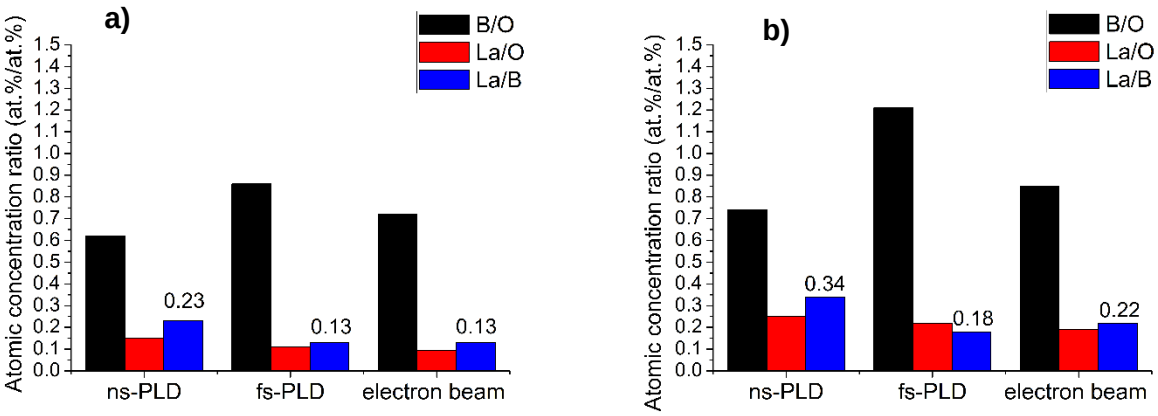

Figure 6: **Atomic ratios of B/O, La/O, and La/B for all the samples, *(a)* before and *(b)* after 30 s of Ar^+ ion sputtering.**

Surface morphologies of the films reported in Table I are shown with the same magnification in **Figure 7.** As expected, the formation of nanoparticles is observed for the fs-PLD sample (**Figure 7b**). The film structure does not appear compact: this could be a detrimental aspect for thermionic emission due to the presence of voids reducing the electrical and thermal conductivity. A nanograined but compact structure characterizes the ns-PLD samples (**Figure 7a**), whereas e^--beam deposition induces the formation of lamelliform nanostructures of irregular sizes but homogeneously distributed.

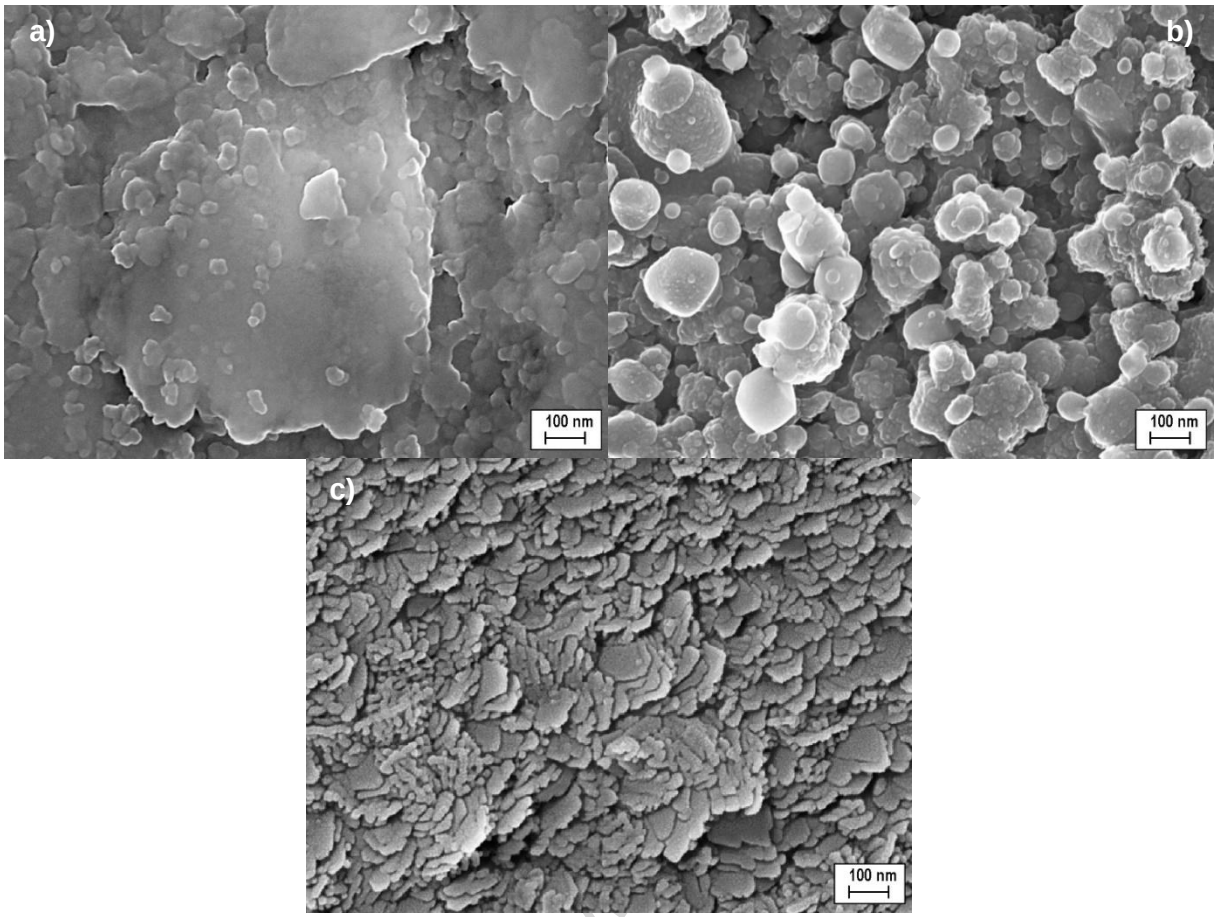

Figure 7: SEM images (250 kX magnification) of a) ns-PLD, b) fs-PLD, and c) e^--beam thin films on tantalum substrates.

3.5 Thermionic electron emission characterization

The thermionic electron emission of the selected films were measured up to 1600 °C. **Figure 8** shows the thermionic saturation current density J_0 as a function of the sample temperature in the range 700 - 1600 °C. The Richardson–Dushman equation $J_0 = A_R T^2 \exp(-\phi/k_B T)$ was used to fit the experimental data [25], where A_R is the effective Richardson constant (A/cm^2K^2) that depends on the material's properties and the reflections at the cathode interfaces, T is the temperature (K), and k_B is Boltzmann's constant. The considerable value of 1.48 A/cm^2 current density is measured at 1600 °C in the fs-PLD sample, connected to an expected emission value of about 40 A/cm^2 at 2000 °C. The work function and the Richardson constant can be obtained by evaluating the slope of the $\ln (J_0/T^2)$ versus T^{-1} plot, according to the method described in [26]. The fit parameters provided for all the samples are compared in **Table II**.

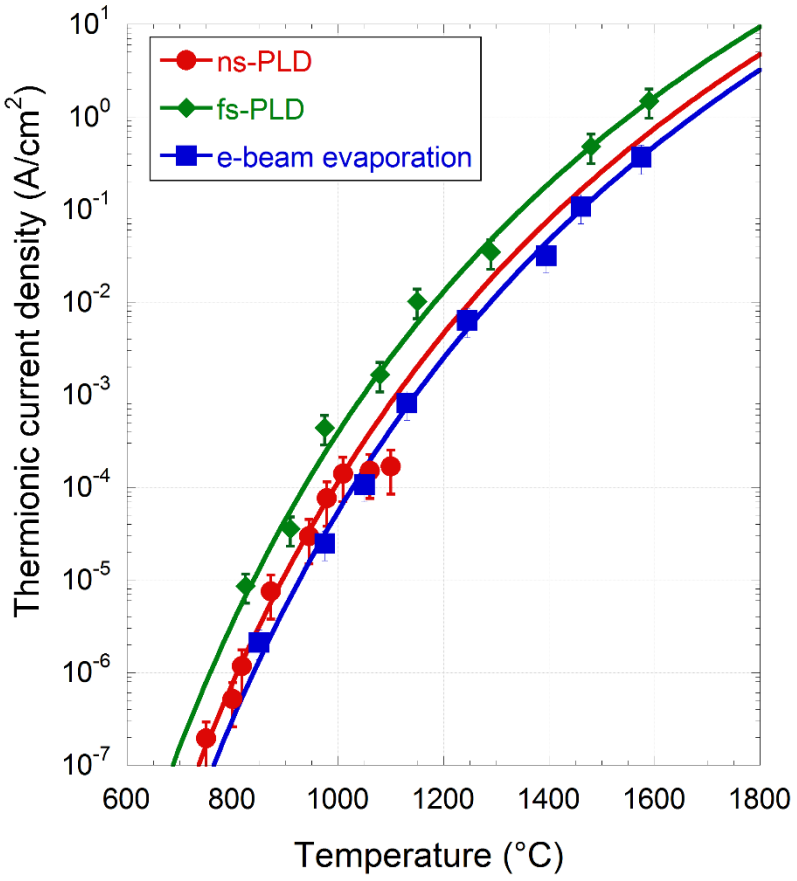

Figure 8: Thermionic current density of samples listed in Table I in the temperature range of 700 — 1600 °C. Continuous lines identify the best fit of the Richardson-Dushman equation applied to the experimental data.

Deposition technique	**ϕ (eV)**	**A_R (A/cm^{2}K^2)**
ns-PLD	2.80 ± 0.18	8.32 ± 2.99
fs-PLD	2.59 ± 0.03	4.31 ± 0.82
e$^-$-beam evaporation	2.85 ± 0.13	6.21 ± 1.75

Table II: Values of work function and Richardson constant of the samples prepared by different techniques and listed in Table I.

The sample deposited by fs-PLD show the lowest work function of 2.59±0.03 eV, coherently with the values reported for LaB_6 thin films. This value is significantly lower than that measured by UPS investigation at RT (3.2 - 3.4 eV). On the other hand, ns-PLD film shows a higher work function value of 2.80±0.18 eV, even if the work function measured by UPS is similar to that of fs-PLD samples. The film deposited by e$^-$-beam evaporation provides the highest work function value of 2.85±0.13 eV, connected to low emission current density. However, it is interesting to notice in Figure 8 that the ns-PLD samples show a deviation from the expected Richardson-Dushman

behavior when the temperature exceeds 1000 °C. This aspect is probably correlated to the desorption of oxides occurring in all the films at high temperatures: in the case of ns-PLD, the degradation of the electron emission is probably due to the thermal decomposition of the predominant oxy-borides crystalline matrix present in the films. To confirm this hypothesis, the desorption monitoring of the chemical species was performed *in situ* by mass spectrometry. The desorption of BO (26 amu), B_2O_2 (54 amu), and B_2O_3 (70 amu) was recorded in the temperature range of 800-1100 °C for all the samples. BO and B_2O_2 fragments could be the products of the B_2O_3 desorption from the film surface [27]. In all the cases, the high temperature induces the evaporation of surface oxides. This effect leads to a reduction of the work function thanks to a cleaner surface, thus explaining the different values of the work function compared with the room-temperature UPS measurements.

Finally, a qualitative consideration has to be tackled about the resulting effective Richardson constant that is a parameter important likewise the work function is. The measured values are more than one order of magnitude lower than the ideal one of 120 A/cm^2K^2. Apart from the oxygen content in the film, it would seem that the compactness of the film mostly influences the Richardson constant, with values passing through 8.32±2.99, 6.21±1.75, and 4.31±0.82 A/cm^2K^2 for films deposited by ns-PLD, e^--beam, and fs-PLD, respectively. This trend seems to be coherent with the analyzed SEM micrographs and reasonable if considering that the dominant effect in the Richardson constant reduction is the electron reflection at the substrate/emitter and emitter/vacuum interfaces. In any case, this aspect needs a significant quantitative deepening in the near future.

Conclusions

Nanocrystalline lanthanum (oxy)boride thin films were obtained by different deposition techniques (ns-PLD, fs-PLD, and electron beam evaporation) for analyzing their thermionic emission capability at high temperatures when deposited on tantalum substrates. The thin films deposited by fs-PLD show the best performance in terms of thermal electron emission, with a work function of 2.59±0.03 eV, a measured current density value of 1.48 A/cm^2 at 1600 °C and an expected emission value of about 40 A/cm^2 at 2000 °C. This result ratifies fs-PLD as the preference method for the preparation of efficient electron emission thin films, with a performance due to a better crystallization of LaB_6, which is the only crystalline phase present in the polycrystalline film. La-B-O crystalline compounds and amorphous structures were revealed the thin films deposited by ns-PLD and electron-beam evaporation, respectively, limiting the temperature operating range and the emission capability.

Acknowledgements

The project AMADEUS has received funds from the European Union's Horizon2020 research and innovation program, FET-OPEN action, under grant agreement 737054. The sole responsibility for the content of this publication lies with the authors. It does not necessarily reflect the opinion of the European Union. Neither the REA nor the European Commission are responsible for any use that may be made of the information contained therein.

The authors thank Ms Alice Fornari for the precious help in the thermionic emission measurements and Mr Marco Guaragno for his technical support with Raman and XRD experiments.

References

[1] T. Bauer, Thermophotovoltaics (Springer, Berlin, Heidelberg, 2011).

[2] G. N. Hatsopoulos and E. P. Gyftopoulos, Thermionic Energy Conversion, Vol. 1: Processes and Devices (The MIT Press, Cambridge, 1973).

[3] G. J. Snyder, E. S. Toberer, Complex thermoelectric materials, Nat. Mater. 7 (2008) 105.

[4] A. Bellucci, et al., Preliminary characterization of ST^2G: Solar thermionic-thermoelectric generator for concentrating systems, AIP Conference Proceedings 1667 (2015) 020007.

[5] D. M. Trucchi, A. Bellucci, M. Girolami, P. Calvani, E.Cappelli, S. Orlando, R. Polini, L. Silvestroni, D. Sciti, and A. Kribus, Solar Thermionic-Thermoelectric Generator (ST^2G): Concept: Materials Engineering, and Prototype Demonstration 8 (2018) 1802310.

[6] J. W. Schwede, et al., Photon-enhanced thermionic emission for solar concentrator systems, Nat. Mater. 9(9), 762–767 (2010).

[7] M. Girolami, L. Criante, F. Di Fonzo, S. Lo Turco, A. Mezzetti, A. Notargiacomo, M. Pea, A. Bellucci, P. Calvani, V.Valentini, D. M. Trucchi, Graphite distributed electrodes for diamond-based photon-enhanced thermionic emission solar cells, Carbon 111 (2017) 48-53.

[8] P. Calvani, A. Bellucci, M. Girolami, S. Orlando, V. Valentini, R. Polini, D.M. Trucchi, Black diamond for solar energy conversion, Carbon 105 (2016) 401.

[9] A. Datas, Hybrid thermionic-photovoltaic converter, Applied Physics Letters 108, 143503 (2016).

[10] R.M.Adams, Boron, Metallo-Boron Compounds, and Boranes, Interscience Publishers, NewYork, 1964.

[11] C.R.Crowell, The Richardson constant for thermionic emission in Schottky barrier diodes, Solid-State Electronics 8(4) (1965) 395-399.

[12] L.W. Swanson, M.A. Gesley and P.R. Davis, Crystallographic dependence of the work function and volatility of LaB_6, Surface Science 107 (1981) 263-289.

[13] A. Yutani, A.Kobayashi, A. Kinbara, Work functions of thin LaB_6 films, Applied Surface Science 70/71 (1993) 737-741.

[14] W. Waldhauser, C. Mitterer, J. Laimer, H. Störi, Structure and electron emission characteristics of sputtered lanthanum hexaboride films, Surf. Coat. Technol. 74-75 (1995) 890-896.

[15] V. Craciun and D. Craciun, Pulsed laser deposition of crystalline LaB_6 thin films, Appl. Surf. Sci. 247 (2005) 384.

[16] A. Mezzi, P. Soltani, S. Kaciulis, A. Bellucci, M. Girolami, M. Mastellone, D. M. Trucchi, Investigation of work function and chemical composition of thin films of borides and nitrides, Surf. Interface Anal. 50 (2018) 1138-1154.

[17] Powder Diffraction File, JCPDS International Center for Powder Diffraction Data, $LaBO_3$, Swarthmore, PA, # 96-220-8747.

[18] Powder Diffraction File, JCPDS International Center for Powder Diffraction Data, B_2O_3, Swarthmore, PA, # 96-201-6173.

[19] M.F. Sunding, K. Hadidi, S. Diplas, O.M. Løvvik, T.E. Norby, A.E. Gunnæs, XPS characterisation of in situ treated lanthanum oxide and hydroxide using tailored charge referencing and peak fitting procedures, J. Electr. Spectrosc. Rel. Phenom. 184 (2011) 399.

[20] V. Craciun et al., Characteristics of LaB_6 thin films grown by pulsed laser deposition, Journal of Vacuum Science & Technology A 34 (2016)051509.

[21] D. J. Late et al., Some aspects of pulsed laser deposited nanocrystalline LaB_6 film: atomic force microscopy, constant force current imaging and field emission investigations, Nanotechnology 19 (2008) 265605.

[22] Lijia Liu, Y. M. Yiu, T. K. Sham, Dongfang Yang, and Lucia Zuin, Electronic structure of nanopolycrystalline pulsed laser deposited films and single crystals LaB_6: The boron perspective, Journal of Applied Physics 107 (2010) 043703.

[23] A. Bellucci, S. Orlando, M. Mastellone, M. Girolami, A. Generosi, B. Paci, A. Mezzi, S. Kaciulis, R. Carducci, R. Polini, and D. M. Trucchi, Low work function nanocrystalline lanthanum boride thin films obtained by femtosecond pulsed laser deposition for efficient electron emitters, submitted to Adv. Func. Mat. (2018).

[24] G. Ausanio, S. Amoruso, A.C. Barone, R. Bruzzese, V. Iannotti, L. Lanotte, M. Vitiello, Production of nanoparticles of different materials by means of ultrashort laser pulses, Applied Surface Science 252 (2006) 4678–4684.

[25] S. Dushman, Thermionic emission, Rev. Mod. Phys. 2 (1930) 381.

[26] F. Jin, and A. Beaver, Barium strontium oxide functionalized carbon nanotubes thin film thermionic emitter with superior thermionic emission capability, Journal of Vacuum Science & Technology B, Nanotechnology and Microelectronics: Materials, Processing, Measurement, and Phenomena 35 (2017) 041202.

[27] J. S. Ozcomert and M. Trenary, Oxide thermal Desorption from the LaB_6 (100) Surface following Reaction with O_2, Chem. Mater. 5 (1993) 1762-1771.

Highlights

- LaB_6-based thin films were grown by ns-PLD, fs-PLD, e^--beam evaporation.
- (Oxy)boride compounds were formed with all the techniques.
- The reduction of oxide species is obtained for fs-PLD.
- fs-PLD induces the achievement of the lowest work function (2.59 eV).